Paramagnetic Carbon-13 and Phosphorus-31 NMR Relaxation Studies of the Stability, Structure, and Dynamics of Complexes in the Glycine/Manganese(II)/Adenosine 5′-Triphosphate System

Jens J. Led

Contribution from the Department of Chemical Physics, University of Copenhagen, the H. C. Ørsted Institute, 5, Universitetsparken, DK-2100 Copenhagen Ø, Denmark.
Received January 24, 1985

Abstract: The paramagnetic relaxation rates, R_{1p} and R_{2p}, of the glycine carbon-13 atoms and the ATP phosphorus-31 atoms of the ternary glycine/Mn^{2+}/ATP^{4-} system at pH 7.4 have been studied as a function of the temperature, magnetic field strength, and glycine and ATP^{4-} concentrations, using a protein-stabilizing solvent consisting of a water–glycerol mixture (3:2, v/v). A subsequent nonlinear least-squares analysis of the data showed that only one ternary glycine–Mn^{2+}–ATP^{4-} complex, $Mn(ATP)(Gly)^{2-}$, is present over a wide range of glycine and ATP^{4-} concentrations. In contrast, a total of *three* consecutive, binary Mn^{2+}–ATP^{4-} complexes, $Mn(ATP)^{2-}$, $Mn(ATP)_2^{6-}$, *and* $Mn(ATP)_3^{10-}$, can be identified in the same ATP^{4-} concentration range, their individual amount being dependent on the ATP^{4-} concentration. Further, the presence of these complexes and especially the latter tris complex reconcile the relaxation data obtained when $[ATP^{4-}] \simeq [Mn^{2+}]$ with those obtained when $[ATP^{4-}] \gg [Mn^{2+}]$. Also, the formation of two binary Mn^{2+}–glycine complexes previously identified was established. The effect of the ligand exchange could be described by generalized equations derived previously. Likewise, the analysis demonstrated that the paramagnetic ^{13}C and ^{31}P relaxations of the metal-bound ligands and the relaxation of the electrons conform closely to the Solomon–Bloembergen–Morgan theories, despite the fact that the basic assumption of the latter theories is barely fulfilled for the scalar relaxation of the glycine $^{13}C(1)$ atom in part of the experimental region. Further, it was found that the data set is sufficiently versatile to allow an unraveling of the relaxation mechanisms as well as an independent evaluation of the pertinent parameters of the applied theoretical model. In particular, the evaluation of the stability constants of the complexes involved allows a determination of absolute values of the distances and hyperfine coupling between the Mn^{2+} ion and the glycine $^{13}C(1)$ or the ATP^{4-} ^{31}P atoms, respectively, as well as a determination of the ligand exchange rates, the electron relaxation rates, and the reorientation rates of the complexes. These parameters, in turn, provide detailed information about the geometry and dynamics of the mixed-ligand glycine–Mn^{2+}–ATP^{4-} complex and the binary Mn^{2+}–ATP^{4-} complexes. Thus, it is found that the glycine of the mixed-ligand complex, in contrast to the glycine of the binary Mn^{2+}–glycine complexes, binds to the Mn^{2+} only through its carboxyl group, leaving the amino group noncoordinated. Likewise, the presence of ATP^{4-} in the first coordination sphere increases the exchange rate of the glycine ligands. On the basis of model building, possible interactions between the amino acid and the nucleotide that can explain these differences are suggested. Finally, the results indicate that the structures of the $Mn(ATP)_2^{6-}$ and $Mn(ATP)_3^{10-}$ complexes are stabilized by stacking interactions between the adenine rings, while the Mn^{2+} ion coordinates to only two phosphate groups of one of the ATP^{4-} molecules and to the N(7) of one of the adenine rings of the complexes.

The importance of mixed-ligand metal ion systems in biological processes, exemplified by many metal-ion-dependent enzyme systems, has triggered numerous studies of low-molecular-weight ternary metal complexes in solution.[1-6] In particular, attention has been focused on interactions between the different ligands and the influence of these interactions on the stability, structure, or formation kinetics of the mixed complexes and their relation to the specificity and selectivity of metal-ion-dependent biological processes.

So far, mainly mixed-ligand complexes of amino acids and organic ligands have been studied,[1-3] using metal ions primarily of the 3d series. Recently, also a few cases of the biologically important amino acid–nucleotide–metal ion complexes were investigated.[4-6] Thus, metal-promoted stacking between nucleoside 5′-triphosphates and aromatic amino acid side chains[4,5] and hydrophobic interactions between ATP^{4-} and aliphatic amino acid side chains[6] have been demonstrated by potentiometric pH titrations and ^1H NMR chemical shifts measurements.

However, aside from the results of these valuable studies, very little information is available about the structure and stability of the complexes being formed in mixed amino acid/nucleotide/metal systems in solution and about their dynamics and formation kinetics. Obviously, this is due to the high complexity of the multicomponent, ternary systems which often requires extensive considerations of all the involved complexes, if detailed information about the individual complexes is to be obtained. This was demonstrated[7] in a preliminary ^{13}C NMR relaxation study of the mechanism of the first step of the protein biosynthesis in which an amino acid is activated through the formation of an aminoacyl adenylate, a reaction that is catalyzed by the cognate aminoacyl-tRNA synthetase[8-11] in the presence of ATP^{4-} and Mg^{2+} or Mn^{2+} ions. Using glycine and the corresponding tRNA synthetase from *E. coli* as an example, it was found that in order to deduce mechanistic features of the activation reaction from NMR relaxation data, precise and detailed information must be provided about the stability and ligand exchange rates, as well as the structure and mobility of all the complexes involved in the

(1) Martin, R. P.; Petit-Ramel, M. M.; Scharff, J. P. In "Metal Ions in Biological System"; Sigel, H., Ed.; Marcel Dekker: New York, 1973; Vol. 2, pp 1–61 and references cited herein.
(2) Sigel, H. In "Metal Ions in Biological Systems"; Sigel, H., Ed.; Marcel Dekker: New York, 1973; Vol. 2, pp 63–125 and references cited herein.
(3) Sharma, V. S.; Leussing, D. L. In "Metal Ions in Biological Systems"; Sigel, H., Ed.; Marcel Dekker: New York 1973; Vol. 2, pp 127–166 and references cited herein.
(4) Orenberg, J. B.; Fischer, B. E.; Sigel, H. *J. Inorg. Nucl. Chem.* **1980**, *42*, 785–792.
(5) Sigel, H.; Naumann, C. F. *J. Am. Chem. Soc.* **1976**, *98*, 730–739.
(6) Sigel, H.; Fischer, B. E.; Farkas, E. *Inorg. Chem.* **1983**, *22*, 925–934.
(7) Led, J. J.; Andersen, A. J. *FEBS. Lett.* **1981**, *124*, 293–298.
(8) (a) Söll, D.; Schimmel, P. B. In "The Enzymes"; Boyer, P. D., Ed.; Academic Press: New York, 1974; Vol. X, pp 489–538. (b) *Ann. Rev.* Biochem. **1979**, *48*, 601–648.
(9) Cole, F. X.; Schimmel, P. R. *Biochemistry* **1970**, *16*, 3143–3148.
(10) Hyafil, F.; Blanquet, S. *Eur. J. Biochem.* **1977**, *74*, 481–493.
(11) Led, J. J.; Switon, K. W.; Jensen, K. F. *Eur. J. Biochem.* **1983**, *136*, 469–479.

0002-7863/85/1507-6755$01.50/0

quarternary glycine/Mn^{2+}/ATP^{4-}/synthetase system.

NMR relaxation studies themselves offer a potential and general source of information about these properties of paramagnetic metal complexes in solution, as the dominating paramagnetic contribution to the relaxation of the ligand nuclei often depends on most, or all, of the properties mentioned. Although these dependencies can become rather entangled, strategies for an unraveling of the individual contributions to the relaxation of the ligand nuclei have been outlined in a series of studies[12-15] of binary paramagnetic complexes.

The present NMR relaxation studies extend these strategies to a ternary amino acid/nucleotide/metal ion system, exemplified by the glycine/Mn^{2+}/ATP^{4-} system at neutral pH. As in previous, related studies,[7,11,15] a mixture of water and glycerol (3:2, v/v) was used as the solvent. Besides acting as a protein-stabilizing medium,[16] this solvent also allows experiments at temperatures below 0 °C,[17] thereby providing an extension of the experimental temperature region necessary for a rigorous analysis of the relaxation data.

The study here also focuses on the difference in nature of the binary Mn^{2+}–ATP^{4-} complexes that dominate at highly different values of the Mn^{2+}/ATP^{4-} ratio. Although the interactions between Mn^{2+} and ATP^{4-} in solution have been the subject of many investigations,[18-24,28] the relation between the monocomplex, $Mn(ATP)^{2-}$, that dominates only at low Mn^{2+} and ATP^{4-} concentrations and those formed at relatively high concentrations of both ions, or with a large surplus of the nucleotide as normally used in NMR studies, has so far remained unclear.[24]

Theoretical Models

In spite of its simplicity compared with in vivo biological systems as, for example, living cells, the system investigated here proves rather intricate. Thus, even though ATP is present mainly as ATP^{4-} at the applied pH of 7.4, and glycine primarily as dipolar ions, at least eight equilibria must be considered.

First, the two binary monocomplexes

$$Mn^{2+} + Gly \rightleftarrows Mn(Gly)^{2+}$$

$$K^{M}_{MG} = \frac{[Mn(Gly)^{2+}]}{[Gly][Mn^{2+}]} \tag{1}$$

and

$$Mn^{2+} + ATP^{4-} \rightleftarrows Mn(ATP)^{2-}$$

$$K^{M}_{MA} = \frac{[Mn(ATP)^{2-}]}{[ATP^{4-}][Mn^{2+}]} \tag{2}$$

are being formed. These complexes are the precursers for the ternary complex

$$Mn(ATP)^{2-} + Gly \rightleftarrows Mn(ATP)(Gly)^{2-}$$

$$K^{MA}_{MAG} = \frac{[Mn(ATP)(Gly)^{2-}]}{[Mn(ATP)^{2-}][Gly]} \tag{3}$$

Further, the two bis complexes

$$Mn(Gly)^{2+} + Gly \rightleftarrows Mn(Gly)_2{}^{2+}$$

$$K^{MG}_{MG_2} = \frac{[Mn(Gly)_2{}^{2+}]}{[Mn(Gly)^{2+}][Gly]} \tag{4}$$

and

$$Mn(ATP)^{2-} + ATP^{4-} \rightleftarrows Mn(ATP)_2{}^{6-}$$

$$K^{MA}_{MA_2} = \frac{[Mn(ATP)_2{}^{6-}]}{[Mn(ATP)^{2-}][ATP^{4-}]} \tag{5}$$

will be present at sufficiently high ligand concentrations[15,20] and can influence the measured relaxation rates. Similar bis complexes have been proposed for other divalent metal ions[25] (Me^{2+} = Mg^{2+}, Ni^{2+}, or Co^{2+}).

Just as stacking between the adenine rings may increase the stability of the $Me(ATP)_2{}^{6-}$ complexes,[20,25] so might the metal ions induce stacking. Indeed, it has been reported[26] that the equilibrium constant for stacking of $Mg(ATP)^{2-}$ is 3 times greater than that of ATP^{4-}. Likewise, stronger interactions among ATP^{4-} molecules in the presence of Mg^{2+} and Ca^{2+} have been suggested from Raman spectroscopic results[27] and in the presence of Zn^{2+} and Cd^{2+} by ^1H NMR chemical shift measurements.[28] Therefore, in solutions with a large surplus of ATP^{4-} compared with the metal ion, it seems reasonable also to expect base-stacked complexes beyond $Mn(ATP)_2{}^{6-}$ and, possibly, beyond $Mn(ATP)(Gly)^{2-}$, that is, complexes in which further ATP^{4-} molecules are attached to the metal complexes through base stacking to ATP^{4-} molecules already bound. Thus, the tris complex $Mn(ATP)_3{}^{10-}$

$$Mn(ATP)_2{}^{6-} + ATP^{4-} \rightleftarrows Mn(ATP)_3{}^{10-}$$

$$K^{MA_2}_{MA_3} = \frac{[Mn(ATP)_3{}^{10-}]}{[Mn(ATP)_2{}^{6-}][ATP^{4-}]} \tag{6}$$

as well as the mixed complex $Mn(ATP)_2(Gly)^{6-}$ may be formed. Finally, metal-free ATP^{4-} molecules may form base stacks, primarily dimers, $(ATP)_2{}^{8-}$, as found in metal-free solutions.[26]

Irrespective of the complexes involved, the following balances must be fulfilled

$$[M]_0 = [M]_{free} + [M]_{complex} \tag{7}$$

and

$$[ATP]_0 = [ATP]_{free} + [ATP]_{complex} \tag{8}$$

where $[M]_0$ and $[ATP]_0$ are the total Mn^{2+} and ATP^{4-} concentrations, respectively, while $[M]_{free}$, $[ATP]_{free}$, $[M]_{complex}$, and $[ATP]_{complex}$ are the concentrations of the corresponding free and complex-bound species. A similar relation for glycine can be ignored when a large surplus of glycine relative to Mn^{2+} is applied, as in the present study.

The influence of the ligand exchanges on the paramagnetic contribution, R_{1p} and R_{2p}, to the measured relaxation rates is given by the general equations[13,15]

$$R_{1p} = \frac{1}{\tau_a} - \sum_{j \neq a} \frac{\mathcal{R}_{aj}|\vec{\mathcal{R}}^{aj}|}{|\vec{\mathcal{R}}^{aa}|} \tag{9}$$

$$R_{2p} = \frac{1}{\tau_a} - \sum_{j \neq a} \mathrm{Re}\left(\frac{\mathcal{S}_{aj}|\vec{\mathcal{S}}^{aj}|}{|\vec{\mathcal{S}}^{aa}|} \right) \tag{10}$$

where the summations are over all paramagnetic sites involved.

(12) Led, J. J.; Grant, D. M. *J. Am. Chem. Soc.* **1975**, *97*, 6962–6970.
(13) Led, J. J.; Grant, D. M. *J. Am. Chem. Soc.* **1977**, *99*, 5845–5858.
(14) Led, J. J. *Mol. Phys.* **1980**, *40*, 1293–1313 and references cited herein.
(15) Led, J. J. *J. Phys. Chem.* **1984**, *88*, 5531–5537.
(16) Schmid, R. D. In "Advances in Biochemical Engineering"; Ghose, T. K., Fiechter, A., Blakebrough, N., Eds.; Springer-Verlag: Berlin, 1979; Vol. 12, pp 41–119. Gekko, K.; Timasheff, S. N. Biochemistry **1981**, *20*, 4667–4686.
(17) Douzou, P. "Cryobiochemistry"; Academic Press: London/New York, 1977.
(18) Cohn, M.; Hughes, T. R., Jr. *J. Biol. Chem.* (a) **1960**, *235*, 3250–3253; (b) **1962**, *237*, 176–181.
(19) Sternlicht, H.; Shulman, R. G.; Anderson, E. W. *J. Chem. Phys.* **1965**, *43*, (a) 3123–3132, (b) 3133–3143.
(20) Sternlicht, H.; Jones, D. E.; Kustin, K. *J. Am. Chem. Soc.* **1968**, *90*, 7110–7118 and references cited herein.
(21) Glassman, T. A.; Cooper, C.; Harrison, L. W.; Swift, T. J. *Biochemistry* **1971**, *10*, 843–851.
(22) Lam, Y.-F.; Kuntz, G. P. P.; Kotowycz, G. *J. Am. Chem. Soc.* **1973**, *96*, 1834–1839.
(23) Kuntz, G. P. P.; Lam, Y.-F.; Kotowycz, G. *Can. J. Chem.* **1975**, *53*, 926–932.
(24) Martin, R. B.; Mariam, Y. H. In "Metal Ions in Biological System"; Sigel, H., Ed.; Marcel Dekker: New York, 1979; Vol. 8, pp 57–124 and references cited herein.
(25) Granot, J.; Fiat, D. *J. Am. Chem. Soc.* **1977**, *99*, 70–79.
(26) Mitchell, P. R.; Sigel, H. *Eur. J. Biochem.* **1978**, *88*, 149–154.
(27) Heyde, M. E.; Rimai, L. *Biochemistry* **1971**, *10*, 1121–1128.
(28) Scheller, K. H.; Hofstetter, F.; Mitchell, P. R.; Prijs, B.; Sigel, H. *J. Am. Chem. Soc.* **1981**, *103*, 247–260.

Further, τ_a^{-1} is the reciprocal lifetime of the ligand in the metal-free state, $|\vec{\mathcal{R}}^{aa}|$ and $|\vec{\mathcal{R}}^{aj}|$ are the determinants of the cofactor matrices of the elements $\mathcal{R}_{aa}$ and $\mathcal{R}_{aj}$, respectively, and $\vec{\mathcal{R}}$ is the sum of the appropriate transition rate and chemical exchange rate matrices. A similar definition holds for the determinants of the corresponding $\vec{\mathcal{S}}$ cofactor matrices.

Although eq 9 and 10 were derived originally[13,15] for the case of one diamagnetic (free ligand), and two paramagnetic sites (complexes) only, they also apply to the general case that includes j different paramagnetic sites, as can easily be verified. Therefore, the present case of at least three or four different paramagnetic sites for glycine, corresponding to eq 1, 3 and 4, and the $Mn(ATP)_2(Gly)^{6-}$ complex can be analyzed by using the same general procedure as in previous studies.[7,13-15] Furthermore, since the exchange of glycine is much faster than that of the considerably more potent ATP^{4-} ligand, and since interchange between the two binary Mn^{2+}–glycine complexes does not affect the experimental relaxation rates,[15] the present system can be treated as a five-site case of the type

that is, exchange takes place only between the free ligand, a, and each one of the paramagnetic species, b, c, d, and e, whereas mutual interchanges between the paramagnetic sites can be neglected. This, in turn, reduces the general equations (9) and (10) to

$$R_{1p} = \frac{1}{\tau_a} - \sum_{j\neq a}\frac{\mathcal{R}_{aj}\mathcal{R}_{ja}}{\mathcal{R}_{aa}} = \sum_{j\neq a}\frac{f_j}{f_a(T_{1j} + \tau_{ja})} \qquad (11)$$

and

$$R_{2p} = \frac{1}{\tau_a} - \sum_{j\neq a}\mathrm{Re}\left(\frac{\mathcal{S}_{aj}\mathcal{S}_{ja}}{\mathcal{S}_{aa}}\right) = \sum_{j\neq a}\frac{f_j}{f_a}\frac{1}{\tau_{ja}}\left[\frac{\left(\frac{1}{T_{2j}} + \frac{1}{\tau_{ja}}\right)\frac{1}{T_{2j}} + \Delta\omega_j^2}{\left(\frac{1}{T_{2j}} + \frac{1}{\tau_{ja}}\right)^2 + \Delta\omega_j^2}\right] \qquad (12)$$

which are the well-known Luz–Meiboom[29] and Swift–Connick[30] equations extended to the case of j paramagnetic sites. In eq 11 and 12, f_a and f_j are the fractions of glycine in the free site and the jth metal-bound site, respectively, while T_{1j}^{-1} ($\equiv R_{1j}$) and T_{2j}^{-1} ($\equiv R_{2j}$), τ_{ja}^{-1}, and $\Delta\omega_j$ are the relaxation rates, the reciprocal lifetime, and the contact shift, respectively, of the glycine nuclei in the jth paramagnetic site.

The individual ligand exchange rates, τ_{ja}^{-1}, are given by the Eyring equation

$$\frac{1}{\tau_{ja}} = \frac{kT}{h}\exp\left(-\frac{\Delta H^{\ddagger}_{ja}}{RT} + \frac{\Delta S^{\ddagger}_{ja}}{R}\right) \qquad (13)$$

while R_{1j} and R_{2j} are expressed by the Solomon–Bloembergen equations[31-33]

$$R_{1j} = \frac{2}{15}\frac{S(S+1)g^2\beta^2\gamma_1^2}{r_j^6}\left[\frac{3\tau_{c,1}}{1+\omega_1^2\tau_{c,1}^2} + \frac{7\tau_{c,2}}{1+\omega_S^2\tau_{c,2}^2}\right] + \frac{2}{3}S(S+1)\left(\frac{A}{\hbar}\right)^2\left[\frac{\tau_{e,2}}{1+\omega_S^2\tau_{e,2}^2}\right] \qquad (14)$$

and

$$R_{2j} = \frac{1}{15}\frac{S(S+1)g^2\beta^2\gamma_1^2}{r_j^6}\left[4\tau_{c,1} + \frac{3\tau_{c,1}}{1+\omega_1^2\tau_{c,1}^2} + \frac{13\tau_{c,2}}{1+\omega_S^2\tau_{c,2}^2}\right] + \frac{1}{3}S(S+1)\left(\frac{A}{\hbar}\right)^2\left[\tau_{e,1} + \frac{\tau_{e,2}}{1+\omega_S^2\tau_{e,2}^2}\right] \qquad (15)$$

The first and second terms in both of these equations account for the dipolar and scalar interactions, respectively, between the unpaired Mn^{2+} electrons and the ligand nuclei. The associated correlation rates $\tau_{c,k}^{-1}$ and $\tau_{e,k}^{-1}$, characterizing the modulation of these interactions, are given by $\tau_{c,k}^{-1} = \tau_R^{-1} + R_{ke} + \tau_{ja}^{-1}$ and $\tau_{e,k}^{-1} = R_{ke} + \tau_{ja}^{-1}$, R_{ke} and τ_R^{-1} being the relaxation rates of the unpaired electrons and the effective isotropic reorientation rate of the Mn^{2+}-bound glycine, respectively, while τ_{ja}^{-1} is the ligand exchange rate (eq 13). Further, $A/\hbar$ is the coupling constant for the scalar interaction between the nuclei of the metal-bound ligands and the unpaired metal electrons, while r_j is the corresponding effective electron–nucleus distance. The remaining symbols have their usual meaning. Finally R_{1e} is given by the Bloembergen-Morgan equation[34]

$$R_{1e} = \frac{\Delta^2}{25}[4S(S+1) - 3]\left[\frac{\tau_v}{1+\omega_S^2\tau_v^2} + \frac{4\tau_v}{1+4\omega_S^2\tau_v^2}\right] \qquad (16)$$

Here τ_v is the associated correlation time and Δ is the zero-field-splitting (ZFS) parameter. The temperature dependences of τ_R and τ_v are given by the Arrhenius expression (k = R, v)

$$\tau_k = \tau_k^0 \exp(E_k/RT) \qquad (17)$$

Since here $\omega_S = 2600\omega_1$, all terms in eq 14 and 15 containing $\omega_S^2\tau_{c,2}^2$ and $\omega_S^2\tau_{e,2}^2$ were neglected. This, of course, is valid only if $R_{2e} \lesssim 10^5 R_{1e}$, and thus $\tau_{c,2} > 10^{-5}\tau_{c,1}$ and $\tau_{e,2} > 10^{-5}\tau_{e,1}$. However, these inequalities hold under any circumstances.[35] Neither can the size of the prefactors in eq 14 invalidate this simplifying condition since $A/\hbar \ll g^2\beta^2\gamma_1^2/r_j^6$ for all practical values of $A/\hbar$ and r_j. The following analyses confirm these conclusions.

Experimental Section

The NMR samples were prepared from equal amounts of 90% [^{13}C-(1)]glycine and 90% [^{13}C(2)]glycine (KOR Inc) or from varying amounts of [^{13}C(1)]glycine and unlabeled glycine (Fluka) and ATP (disodium salt, vanadium free, Sigma). Mn^{2+} was obtained as analytical reagent $MnCl_2{\cdot}4H_2O$ (Alfa). Glycine and ATP were used without further purification, whereas the manganese salt was dried in vacuo at 220 °C until the water of crystallization was expelled. The applied solvent, consisting of a mixture of H_2O–glycerol (3:2, v/v), was buffered at pH 7.4 with 20 mM sodium phosphate. In addition, 2-mercaptoethanol (5 mM) was added as in previous, related studies,[7,11,15] due to its stabilizing effect on proteins. In this solvent the two highest pK_a values of the ATP phosphate were found to be 4.4 and 6.9, respectively, by potentiometric titration. The applied 8-mm (OD) NMR tubes, containing 2 mL of sample, were sealed off in vacuo at a length of 8–10 cm to assure a uniform temperature in the samples during the experiments and coaxially mounted in 10-mm (OD) NMR tubes with the lock substance, D_2O, contained in the annulus between the two tubes. The ^{13}C and ^{31}P equilibrium spectra showed no sign of impurities or degradation of the samples within the time of the experiments.

The ^{13}C NMR measurements were accomplished at 67.89 and 22.63 MHz by using Bruker HX 270 and WH 90 spectrometers, respectively, as described previously.[14] The ^{31}P data were obtained at 36.4 MHz by using a JEOL FX 90Q spectrometer employing a 20-μs 90° pulse and 2048 data points to define the 3-kHz spectral range. A broad-band proton decoupling of 1–2 W was used in all cases. The temperature was measured before and after each experiment, using an acetone-d_6/CCl_4

(29) Luz, Z.; Meiboom, S. *J. Chem. Phys.* **1964**, *40*, 2686–2692.
(30) Swift, T. J.; Connick, R. E. *J. Chem. Phys.* **1962**, *37*, 307–320; **1964**, *41*, 2553–2554.
(31) Solomon, I. *Phys. Rev.* **1955**, *99*, 559–565.
(32) Solomon, I.; Bloembergen, N. *J. Chem. Phys.* **1956**, *25*, 261–266.
(33) Reuben, J.; Reed, G. H.; Cohn, M. *J. Chem. Phys.* **1970**, *52*, 1617.
(34) Bloembergen, N.; Morgan, L. O. *J. Chem. Phys.* **1961**, *34*, 842–850.
(35) Rubinstein, M.; Baram, A.; Luz, Z. *Mol. Phys.* **1971**, *20*, 67–80.

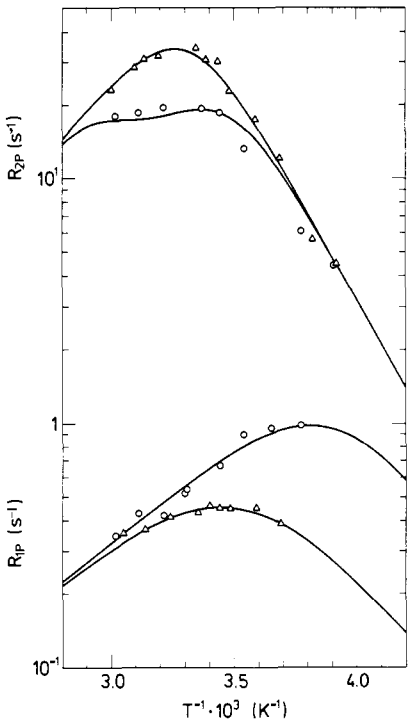

Figure 1. Temperature variation of the Mn^{2+}-induced paramagnetic contributions, R_{2p} and R_{1p}, to the relaxation rates of the glycine $^{13}C(1)$ atom at 67.89 MHz (△) and 22.63 MHz (○). The rates were obtained from a sample containing 0.200 M glycine, 40 mM ATP^{4-}, and 50 μM Mn^{2+}. A H_2O–glycerol mixture (3:2, v/v), 5 mM in 2-mercaptoethanol and buffered at pH 7.4 with a 20 mM sodium phosphate buffer, was used as the solvent. The upper two data sets are the R_{2p} rates, while the lower two sets are the R_{1p} rates. The curves were calculated from the parameters in Tables I, corresponding to the best nonlinear least-squares fit to the data in Figures 1–3 and the R_{2p} data in Figure 4 (see text).

thermometer[36] in the ^{13}C experiments and a normal alcohol thermometer in the ^{31}P experiments. Both thermometers were immersed in 2 mL of the applied buffer in a 10-mm NMR tube. In contrast to previous observations in water solutions,[36] the applied broad-band proton decoupling caused only minor heating effects (<2 °C) in the solvent and samples used here. Also, the temperatures were independent of the glycine and ATP concentrations over the ranges employed.

The experimental R_1 relaxation rates were obtained with the T_{Rep}–180°–τ–90° pulse sequence and extracted from the peak heights of 20–25 partially relaxed Fourier transform spectra by a nonlinear three-parameter least-squares procedure.[14] The 1σ standard deviations of the resulting R_1 values were <2% for ^{13}C and <5% for ^{31}P where average values of the rates of the individual lines in the ^{31}P multiples were employed whenever a multiplet was observable (Mn^{2+}-free sample and Mn^{2+}-containing samples at the lowest temperatures). No paramagnetic effect was observed on the $R_{1,obsd}[^{31}P]$ rates of the phosphate buffer also measured in the ^{31}P experiments. Likewise, the relatively small $R_{1,obsd}$-$[^{31}P]$ rates of ATP^{4-} observed in the metal-free sample (Tables VI–VIII in the supplementary material) guarantee that no significant amount of paramagnetic impurities is present. The ^{13}C R_2 rates were obtained from the line width of the NMR signals, with an estimated uncertainty of 1.5 s^{-1}. In all experiments, a sensitivity enhancement filtering of 5 Hz was applied. The paramagnetic contributions, R_{kp} (k = 1, 2), to the observed relaxation rates, $R_{k,obsd}$, of the ligand nuclei were calculated as $R_{kp} = R_{k,obsd} - R_{ka}$, the only difference between the two rates being the influence from the Mn^{2+} ions on $R_{k,obsd}$, thereby eliminating contributions from relaxation mechanisms other than those due to the presence of the paramagnetic metal ions. $R_{1,obsd}$ and R_{1a} were obtained from corresponding Mn^{2+}-containing and Mn^{2+}-free solutions, respectively, while $R_{2,obsd}$ and R_{2a} were derived from the same spectrum, using the line width of the glycerol $^{13}C(2)$ signal for the R_{2a} determination instead of the line width of the glycine $^{13}C(1)$ signal in a Mn^{2+}-free sample. The latter procedure was justified by the facts that no paramagnetic effect was observed on the R_1 and R_2 relaxation rates of the glycerol carbons in the Mn^{2+}-containing samples and that the line widths of the glycerol $^{13}C(2)$ and the glycine $^{13}C(1)$ signals in a Mn^{2+}-free sample were identical within the experimental uncertainties. In turn, the applied procedure provides R_{2p} values that are unaffected by field inhomogeneities.

(36) Led, J. J.; Petersen, S. B. *J. Magn. Reson.* **1978**, *32*, 1–17.

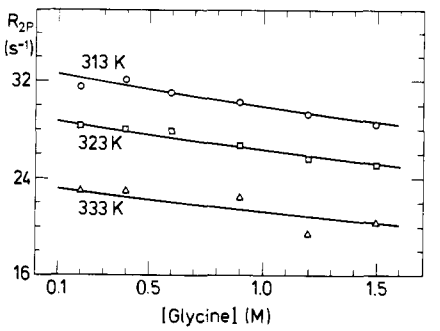

Figure 2. Variation with glycine concentration of the Mn^{2+}-induced paramagnetic contribution, R_{2p}, to the spin–spin relaxation rate of the glycine $^{13}C(1)$ atom at 67.89 MHz and at three different temperatures: 313, 323, and 333 K. The glycine concentrations were as specified, while the ATP^{4-} concentration was 40 mM and the Mn^{2+} concentration was 50 μM. The solvent and buffer were as specified in the legend of Figure 1. The curves were calculated from the parameters in Table I, corresponding to the best nonlinear least-squares fit to the data in Figures 1–3 and the R_{2p} data in Figure 4 (see text).

Results and Discussion

A. Glycine ^{13}C Relaxation Data. Qualitative Evaluation. The R_{1p} and R_{2p} relaxation rates of the glycine C(1) atom were measured as function of the temperature and field strength as shown in Figure 1. Like the corresponding rates of the binary Mn^{2+}/glycine subsystem,[15] those observed here vary considerably with both variables, indicating pronounced dependences on the dynamics and structures of the glycine complexes involved.

Thus, the negative slope at the lowest temperatures shows that here the slow-to-intermediate-exchange condition prevails, implying that the R_{2p} rates are directly dependent on the glycine exchange rate τ_{ja}^{-1}. In contrast, the fast-exchange condition controls the R_{2p} rates at the higher temperatures and the R_{1p} rates in the entire experimental temperature region, showing that the data here depend on the relaxation rates, R_{2j}, and R_{1j}, respectively, of the metal-bound glycine. Likewise, the possibility of determining the effective correlation rates, $\tau_{c,1}^{-1}$ and $\tau_{e,1}^{-1}$, of the R_{2j} and R_{1j} relaxations (eq 14 and 15) is evidenced by the substantial field dependences of both R_{2p} and R_{1p}. Moreover, the observed increase in R_{2p} (R_{2j}) with increasing field strength can be accomplished only if the correlation rate itself is field-dependent. Among the contributions to $\tau_{e,1}^{-1}$ and $\tau_{c,1}^{-1}$, only R_{1e} has this quality and only if $\omega_S^2\tau_v^2 \geq 1$, that is, if the nonextreme narrowing condition applies to the electron relaxation (eq 16). Consequently, information about the electron relaxation can be obtained from the data. Opposite R_{2p}, the R_{1p} rate decreases with increasing field strength in particular at the lowest temperatures, showing that $\omega_1^2\tau_{c,1}^2 \geq 1$; that is, the nonextreme narrowing condition applies to the R_{1j} rates, allowing $\tau_{c,1}^{-1}$ as well as the Mn^{2+}–C(1) distance to be determined if the fraction of metal-bound glycine is known (vide infra). Finally, as explained in details in the case of the binary Mn^{2+}/glycine system,[15] the fact that the inequalities $R_{2p} \gg R_{1p}$ and, thereby, $R_{2j} \gg R_{1j}$ still hold even when the field dependences of both rates are about to disappear at the highest temperatures leads to the conclusions that R_{2j} is controlled by its scalar term, whereas R_{1j} is dominated by its dipolar contribution.

In order to determine the fractions, f_j, of the glycine bound to Mn^{2+} in each one of the individual Mn^{2+} complexes in which glycine participates, additional measurements were made of the R_{2p} rates of the glycine C(1) atom as a function of the glycine concentration at three different temperatures (Figure 2). These data, however, only provide information about the total fraction, P_M, of Mn^{2+}-bound glycine and the associated effective equilibrium constant for the glycine–Mn^{2+} interaction. Therefore, corresponding measurements as a function of the ATP^{4-} concentration (Figure 3) were made in order to account specifically for the binary ATP^{4-}–Mn^{2+} complexes (eq 2 and 5) and the mixed glycine–ATP^{4-}–Mn^{2+} complexes (eq 3). Further, a distinction between

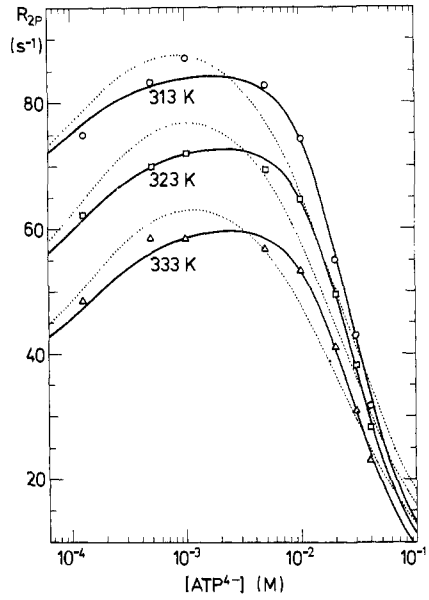

Figure 3. Variation with ATP^{4-} concentration of the Mn^{2+}-induced paramagnetic contribution, R_{2p}, to the spin–spin relaxation rate of the glycine $^{13}C(1)$ atom at 67.89 MHz and at three different temperatures: 313, 323, and 333 K. The ATP^{4-} concentrations were as specified, while the glycine concentration was 200 mM and the Mn^{2+} concentration was 50 μM. The solvent and buffer were as specified in the legend of Figure 1. The full curves were calculated from the parameters in Table I, corresponding to the best nonlinear least-squares fit to the data in Figures 1–3 and the R_{2p} data in Figure 4 (see text). The dotted curves correspond to a model in which the $Mn(ATP)_3^{10-}$ complex was not included (see text).

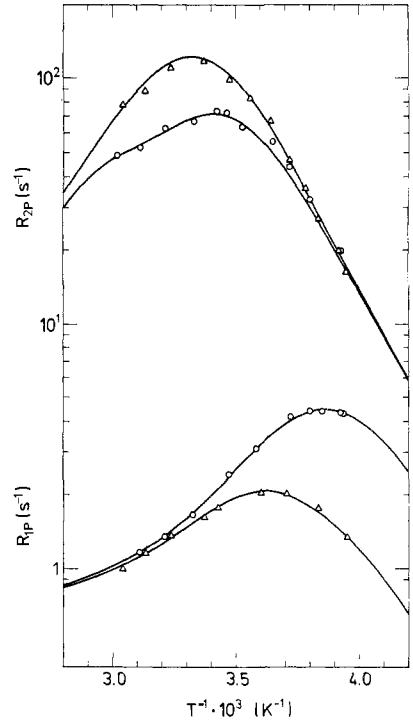

Figure 4. Temperature variation of the Mn^{2+}-induced paramagnetic contribution, R_{2p} and R_{1p}, to the relaxation rates of the glycine $^{13}C(1)$ atom at 67.89 (△) and 22.63 MHz (○). The rates were obtained from a sample containing 0.250 M glycine, 125 μM ATP^{4-}, and 75 μM Mn^{2+}. The solvent and buffer were as specified in the legend of Figure 1. The curves were calculated from the parameters in Table I, corresponding to the best nonlinear least-squares fit to the data in Figures 1–4 (see text).

these complexes was achieved by varying the ATP^{4-} concentration more than 2 orders of magnitude, thereby allowing the individual complexes to dominate in different regions. Also, the two binary Mn^{2+}–glycine complexes (eq 1 and 4) were considered specifically in the analysis, using the parameters derived for these complexes[15] under similar experimental conditions as applied here. Again, the R_{1p} rates of the C(1) atoms of the binary Mn^{2+}–glycine complexes were described by the Burnett–Roeder model,[15,37] which reproduces the apparent anisotropic behavior of these rates caused by an increasing amount of bidentate Mn^{2+}–glycine chelates with temperature. Finally, the effect of the ATP^{4-} concentration on the relaxations of the C(1) atom of glycine bound in the mixed glycine–Mn^{2+}–ATP^{4-} complexes was monitored, by supplementing the data set with the C(1) relaxation rates obtained previously[7] as a function of temperature and field strength under the same experimental conditions (solvent, pH) as the data in Figure 1 when using a comparable Mn^{2+} concentration (75 μM) but at an ATP^{4-} concentration (125 μM) that is 320 times smaller than here. These relaxation rates and their variation with temperature are shown graphically in Figure 4.

B. Quantitative Analysis of the Glycine ^{13}C Relaxation Data. The data were analyzed by fitting the parameters of the model described in the Theoretical Models section. The analysis was performed as in previous studies[7,12-15] using a nonlinear least-squares procedure. The best fit was defined by the usual standard criterion,[38] that is, by the minimum value of the standard deviation, σ, of the measurement error distribution. Calculations from eq 1–8, of the concentrations of the individual complexes and the unbound Mn^{2+} and ATP^{4-}, were performed iteratively by means of the Newton–Raphson procedure.[39] The individual data points were weighted with the reciprocal of their estimated uncertainties.

Prior to the analyses of the total data set, calculations based on part of the data were performed in order to obtain preliminary values of specific parameters. Thus, for example, a preliminary evaluation of $\Delta H^{\ddagger}_{MAG}$ and $\Delta S^{\ddagger}_{MAG}$ can be obtained from the temperature variations of the R_{2p} data at the lowest temperatures and the highest field (Figures 1 and 4). Likewise, provisional estimates of the stability constants, K^{MA}_{MAG}, K^{M}_{MA}, and $K^{MA}_{MA_2}$, can be obtained from the data in Figures 2 and 3, alone. The stability constants were expressed by the modified equation

$$K = \exp\left[-\frac{\Delta H}{R}\left(\frac{1}{T} - \frac{1}{T_0}\right) + \frac{\Delta S'}{R}\right] \qquad (18)$$

where the temperature of reference, T_0, was chosen within the experimental temperature range. This procedure minimizes the, otherwise, strong correlation between the two parameters to be determined (ΔH, $\Delta S'$), leading to more accurate values for these parameters and K, but leaves the entropy of complexation, ΔS, undetermined.

The data in Figures 1–3 were first analyzed by using a model (case I) that includes only the mixed complex, $Mn(ATP)(Gly)^{2-}$ (eq 3), the two binary glycine complexes, (eq 1 and 4), and the binary $Mn(ATP)^{2-}$ complex (eq 2). However, neither this model nor a model (case II) that also includes the $Mn(ATP)_2^{6-}$ complex (eq 5) can describe, simultaneously, the variation with temperature, field strength, and concentration displayed by the data in Figures 1–3. Although the latter model fits the data in Figures 1 and 2, simultaneously, systematic deviations result in the case of the ATP^{4-} titration data, as shown by the dotted curves in Figure 3. In addition, a Mn^{2+}–C(1) distance (3.40 ± 0.11 Å) is obtained, which is incompatible with the direct coordination of the glycine carboxyl group suggested by the large Mn^{2+}–C(1) scalar interaction (R_{2p}).

The deviations indicated by the dotted curves in Figure 3 immediately show that the access of the glycine to the first coordination sphere of the Mn^{2+} ions is more restricted at the lowest and the highest ATP^{4-} concentrations than predicted by the model (case II), while less restricted at the intermediate ATP^{4-} con-

(37) Burnett, L. J.; Roeder, S. B. W. *J. Chem. Phys.* **1974**, *60*, 2420–2423.
(38) Albritton, D. L.; Schmeltekopf, A. L. In "Molecular Spectroscopy, Modern Research"; Rao, K. N., Mathews, C. W., Eds.; Academic Press: New York, 1976; Vol. 2, pp 1–67.
(39) Margenau, H.; and Murphy, G. M. "The Mathematics of Physics and Chemistry", 2nd ed.; D. Van Nostrand: Princeton, NJ, 1956; Vol. 1, pp 492–494.

Table I. Parameters Calculated[a] from the Experimental R_{1p} and R_{2p} Relaxation Rates of the Glycine $^{13}C(1)$ Carbon in the ATP-Containing Samples[b]

ΔH^{MA}_{MAG}, kcal mol^{-1}	0.6 ± 0.2	τ_v^{-1} (298 K), s^{-1}	(2.4 ± 0.3) × 10^{11}
K^{MA}_{MAG} (298 K), mol^{-1}	0.31 ± 0.07	Δ, G	157 ± 22
ΔH^{M}_{MA}, kcal mol^{-1}	−7.4 ± 1.4	R_{1e} (298 K, 21.1 kG), s^{-1}	(2.7 ± 0.6) × 10^7
K^{M}_{MA} (298 K), mol^{-1}	(5.3 ± 0.9) × 10^4	A/h, Hz	(1.3 ± 0.3) × 10^6
$\Delta H^{MA}_{MA_2}$, kcal mol^{-1}	3 ± 3	40 mM ATP[c]	
$K^{MA}_{MA_2}$ (298 K), mol^{-1}	8 ± 3	E_R, kcal mol^{-1}	4.3 ± 0.3
$\Delta H^{MA_2}_{MA_3}$, kcal mol^{-1}	−3 ± 3	τ_R^{-1} (298 K), s^{-1}	(5.8 ± 0.2) × 10^8
$K^{MA_2}_{MA_3}$ (298 K), mol^{-1}	112 ± 50	r[Mn^{2+}–$^{13}C(1)$], Å	3.03 ± 0.10
$\Delta H^{\ddagger}_{MAG}$, kcal mol^{-1}	7.18 ± 0.17	0.125 mM ATP[c]	
$\Delta S^{\ddagger}_{MAG}$, cal mol^{-1} deg^{-1}	−2.8 ± 0.7	E_R, kcal mol^{-1}	6.4 ± 0.2
τ_{MAG}^{-1} (298 K), s^{-1}	(8.2 ± 1.7) × 10^6	τ_R^{-1} (298 K), s^{-1}	(10.0 ± 0.4) × 10^8
E_v', kcal mol^{-1}	9.4 ± 1.0	r[Mn^{2+}–$^{13}C(1)$], Å	2.97 ± 0.09

[a] Case III (see text) including 1σ confidence limits. [b] For sample specification, see captions of Figures 1–4. [c] See text.

centrations. Admittedly, the stability constants of the complexes could be influenced by the variation of the ionic strength with increasing ATP^{4-} concentration. Thus, it has been reported[1] that the stability of ternary metal ion complexes of amino acid anions may increase at high ionic strengths ($\mu > 0.7$), if they carry the same charge as the binary complexes, whereas the stability decreases if changes of the charge occur. However, here the ionic strengths of the solutions are considerably smaller than 0.7 even at the highest ATP^{4-} concentration ($\mu \simeq 0.52$). Moreover, even though the charge of the mixed-ligand complex is different from that of the binary Mn^{2+}–glycine complexes, the observed deviations (Figure 3) are incompatible with a simple decrease of K^{MA}_{MAG}, or any other of the equilibrium constants involved, with increasing ATP^{4-} concentration neither qualitatively nor quantitatively. In this context, it should also be noted that the experimental R_{2p} rates are independent of the diffusional reorientation rates of the molecules (vide infra) and thus unaffected by any changes in the viscosity caused by the changes of the ATP^{4-} concentration.

More likely, therefore, the observed deviations are caused by the presence of additional complexes not accounted for so far. Indeed, an extension of the applied model (case III) by the $Mn(ATP)_3^{10-}$ complex (eq 6) supports this suggestion. As shown by the full curves in Figures 1–3, an excellent fit to all three data sets is now obtained. That also includes the R_{1p} data (Figure 1) which, therefore, conform to the simple isotropic reorientation implied by the Solomon model[31] (eq 14). This contrasts the behavior of the R_{1p} data of the binary Mn^{2+}–glycine complexes,[15] where the data analysis showed that an apparent conflict with the isotropic reorientation model was caused by the formation of an increasing amount of a bidentate glycine–Mn^{2+} chelate with increasing temperature. The simpler temperature dependence of R_{1p} found here suggests that a single, mixed glycine–Mn^{2+}–ATP^{4-} complex dominates in the observed temperature range.

Moreover, the extended model (case III) and the parameters that fit the data in Figures 1–3, also accommodate the R_{2p} data obtained previously at the low ATP^{4-} concentration,[7] as shown in Figure 4. Hence, the relaxation rate, R_{2j}, of the C(1) atom of glycine bound in the mixed complexes and the corresponding glycine exchange rate, τ_{MAG}, are unaffected by the variation in the ATP^{4-} concentration over the applied range from 0.125 to 40 mM, indicating that no significant change of the glycine–Mn^{2+} interaction in the mixed complexes occurs over that ATP^{4-} concentration range. The parameter values obtained from the simultaneous analysis of the data in Figures 1–3 and the R_{2p} data in Figure 4 are given in Table I, while the temperature variation of the correlation rates are shown graphically in Figure 5.

Only the R_{1p} data at the low ATP^{4-} concentration (Figure 4) do not agree with the parameter values obtained in case III. However, when allowing for an independent set of reorientation parameters (τ_R^{-1}, E_R; Table I) for the mixed complex at the low ATP^{4-} concentration, these data also fit in with the rest of the data set and the applied model, including the isotropic reorientation, the Mn^{2+}–C(1) distance, and the remaining parameters in Table I, as shown by the R_{1p} curves in Figure 4. In fact, a better fit to the R_{1p} data in Figure 4 is obtained here where both of the two binary Mn^{2+}–glycine complexes[15] and the temperature variation of their ratio are taken into account specifically than in the previous analysis[7] of these data where no specific allowances were made for the binary Mn^{2+}–glycine complexes.

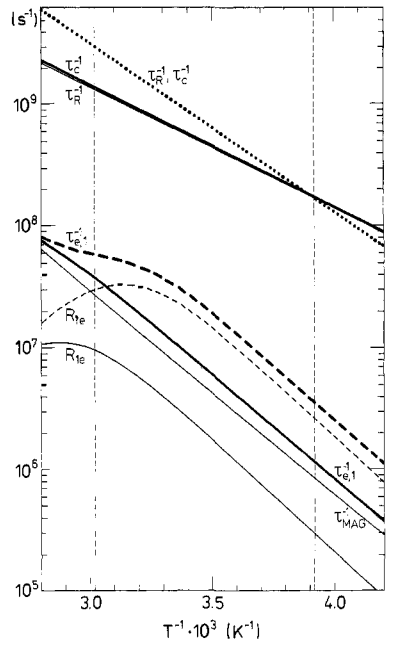

Figure 5. Temperature variation of the effective molecular reorientation rate, τ_R^{-1}, at [ATP^{4-}] = 40 mM (—) or 125 μM (···), the electron relaxation rates, R_{1e}, the glycine exchange rates, τ_{MAG}^{-1}, and the sum of these rates, $\tau_{c,1}^{-1}$ ($=\tau_R^{-1} + \tau_{MAG}^{-1} + R_{1e}$) and $\tau_{e,1}^{-1}$ ($=\tau_{MAG}^{-1} + R_{1e}$), at 67.89 (—) and 22.63 MHz (– – –). The dotted, vertical lines indicate the experimental temperature region. The curves were calculated from the parameters in Table I, corresponding to the best nonlinear least-squares fit to the data in Figures 1–4.

The difference in mobility of the mixed-ligand complexes at the two extremes of the ATP^{4-} concentration range thus established (Table I, Figure 5) could reflect the formation of an increasing amount of $Mn(ATP)_2(Gly)^{6-}$ with increasing ATP^{4-} concentration. This possibility was explored by a fourth data analysis (case IV) in which case III was extended by the latter complex, assuming identical R_{2j} relaxation rates and ligand exchange rates, τ_{MAG}^{-1}, for both mixed complexes. However, no improvement of the fit was obtained by this extension, just as the parameter values derived are identical with those in case III, within the uncertainties. This also includes $K^{MA_2}_{MA_2G}$, which agrees closely with the value of K^{MA}_{MAG}. Thus, except for the reorientation rates, the parameters that

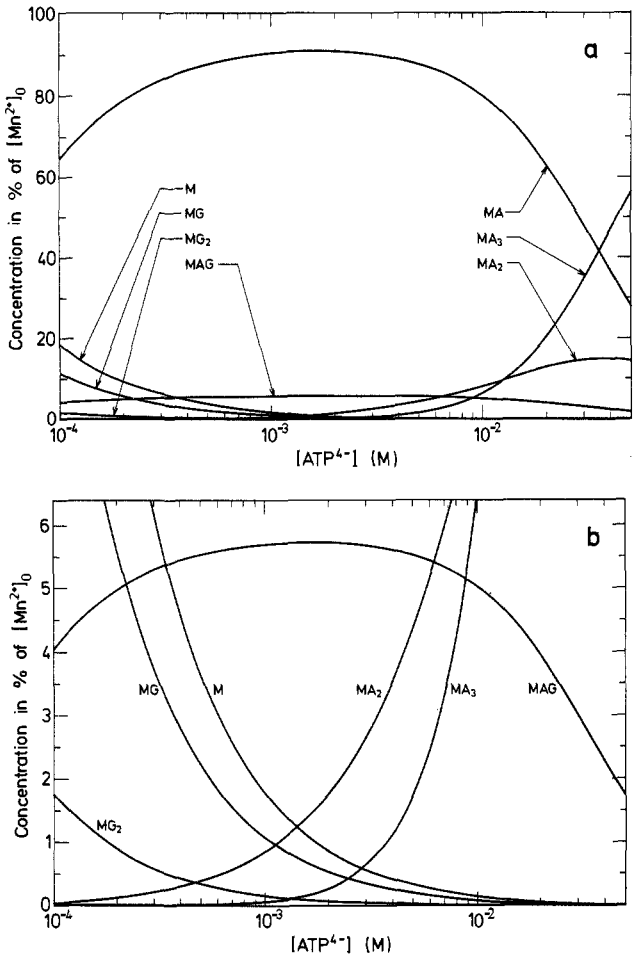

Figure 6. Calculated variation with ATP^{4-} concentration of the composition of the glycine/Mn^{2+}/ATP^{4-} system at pH 7.4 and 298 K. The remaining experimental conditions were as specified in the legend of Figure 1. The total composition is given in a, while b is an expansion showing the less abundant species. M, MG, and MG_2 designate the free Mn^{2+} and the two consecutive, binary Mn^{2+}–glycine complexes. MA, MA_2, MA_3, and MAG are the three consecutive, binary Mn^{2+}–ATP^{4-} complexes and the ternary glycine–Mn^{2+}–ATP^{4-} complexes, respectively. The curves were calculated (eq 1–8) from the stability constants in Table I and the total concentrations of Mn^{2+}, glycine, and ATP^{4-}.

describe the relaxation, the ligand exchange, and the stability of the glycine C(1) atom in the alleged $Mn(ATP)_2(Gly)^{6-}$ complex are identical with those associated with $Mn(ATP)(Gly)^{2-}$, within the uncertainties. Most likely, therefore, the difference in the reorientation rate of the mixed complexes at the two extremes of the ATP^{4-} concentration merely reflects a viscosity effect, rather than a genuine change in the structure and composition of the mixed-ligand complexes.

Finally it should be noted that an extension of the model used in case II (eq 1–5) that includes the $Mn(ATP)_2(Gly)^{6-}$ complex, but not the $Mn(ATP)_3^{10-}$ complex, does not improve the quality of the fit over that obtained in case II (the dotted curves in Figure 3). Likewise, the inclusion of the ATP^{8-} dimers using a realistic dimerization constant,[26] K_D, of 1.3 mol^{-1} has no effect on the fit or the parameter values within the experimental errors.

The composition of the system as a function of the applied glycine and ATP^{4-} concentrations, respectively, calculated from the equilibrium constants in Table I (case III) by using eq 1–8 is given in Figure 6.

C. Carbon-13 Relaxation of the Metal-Bound Glycine. As it appears from Figure 5, the reorientation rate, τ_R^{-1}, controls the correlation rate, $\tau_{c,1}^{-1}$, of the dipolar contributions to the ^{13}C relaxations, R_{1j} and R_{2j}, of the glycine bound in the mixed-ligand complexes, while the electron relaxation rate, R_{1e}, and the ligand exchange rate, τ_{MAG}^{-1}, both contribute to the effective correlation rate, $\tau_{e,1}^{-1}$, for the corresponding scalar interaction. Further, the

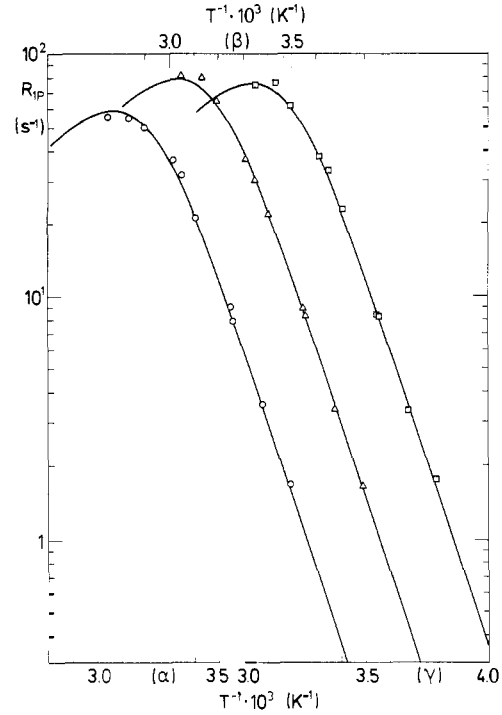

Figure 7. Temperature variation of the Mn^{2+}-induced paramagnetic contribution, R_{1p}, to the relaxation rates of the α-^{31}P (○), β-^{31}P (△), and γ-^{31}P (□) atoms of ATP^{4-} at 36.4 MHz. The rates were obtained from the same sample as in Figure 1. The curves were calculated from the parameters in Tables I and II, corresponding to the best nonlinear least-squares fit to the data in Figures 1–4 and 7.

basic condition,[34,40] $R_{1e} \ll \tau_v^{-1}$, for the validity of the applied Solomon–Bloembergen–Morgan relaxation theories (the Redfield limit) is fulfilled (Table I) in the case of the electron relaxation. These results closely parallel those found previously for the binary Mn^{2+}–glycine complexes.[15]

A quantitative evaluation of R_{1j} (eq 14) using the parameters in Table I confirms that also for this relaxation rate is the basic assumption ($R_{1j} \ll \tau_R^{-1}$) fulfilled. Likewise, it shows that the R_{1j} rate is dominated by the dipolar term over the entire ATP^{4-} concentration range, in agreement with the qualitative conclusion made in section A. Further, a quantitative evaluation of R_{2j} (eq 15) confirms the prediction (section A) that this rate is dominated by its scalar relaxation. However, in the lower part of the temperature region, it is found that $R_{2j} \simeq \tau_{e,1}^{-1}$, in particular at the highest field strength; that is, the scalar relaxation rate is here just at the verge of the Redfield limit. Therefore, the spins may not dephase entirely by a random walk but are partly dephased before their magnetic environments change either due to exchange (τ_{ja}^{-1}) or because of the relaxation (R_{1e}) of the nearby unpaired electrons. If so, the R_{2j} relaxation will increase, exceeding the value predicted by the applied theory, and will approach a solid-state value.[41] Yet, the Redfield limit is only barely touched and only in the lower part of the experimental temperature region where the experimental R_{2p} rate is mostly influenced by the ligand exchange. Therefore, only minor errors in the analysis can occur. This conclusion is supported by the excellent fit (section B) obtained based on the applied theoretical model at both of the magnetic field strengths employed, as well as by the physical reasonableness of the parameters obtained in the analysis (vide infra).

D. ^{31}P Relaxation Data. While the glycine ^{13}C relaxation data determine the stability of the binary Mn^{2+}–ATP^{4-} complexes because of the mutual competition between the two ligands as illustrated above, the R_{1p} rates of the ^{31}P nuclei of ATP^{4-} (Figure 7), obtained as function of temperature at 36.4 MHz and $[ATP^{4-}]$

(40) Redfield, A. G. *Adv. Magn. Reson.* **1965**, *1*, 1–32.
(41) Slichter, C. P. "Principles of Magnetic Resonance"; Harper and Row: New York, 1963; pp 155–156.

Table II. Parameters[a] Calculated from the Experimental R_{1p} Relaxation Rates of the Phosphorus Atoms of ATP^{4-} in a Glycine-Containing Sample[b]

$\Delta H^{\ddagger}_{ATP}$, kcal mol^{-1}	13.57 ± 0.13
$\Delta S^{\ddagger}_{ATP}$, cal mol^{-1} deg^{-1}	7.4 ± 0.5
τ_{ATP}^{-1} (298 K), s^{-1}	(2.82 ± 0.05) × 10^4
$r[Mn^{2+}-{}^{31}P_{\alpha}]$, Å	3.54 ± 0.05
$r[Mn^{2+}-{}^{31}P_{\beta}]$, Å	3.32 ± 0.07
$r[Mn^{2+}-{}^{31}P_{\gamma}]$, Å	3.36 ± 0.05

[a] Including 1σ confidence limits. [b] See captions of Figures 1 and 8 for sample specifications.

= 40 mM, provide information about the structure of the Mn^{2+}–ATP^{4-} complexes and the ATP^{4-}–ligand exchange rate.

As seen in Figure 7, the R_{1p} rates of all three ^{31}P nuclei of ATP^{4-} are in the slow-exchange region at the lower experimental temperatures and are, therefore, controlled by the ATP^{4-}–ligand exchange rate, τ_{ATP}^{-1}, at these temperatures. On the other hand, the influence of the relaxation rates, R_{1j}, of the Mn^{2+}-bound ATP^{4-} is significant at the highest temperatures as evidenced by the temperature dependences in this region. Hence, distance information can be obtained.

A quantitative analysis of the ^{31}P relaxation data was performed, using some of the results obtained in the analysis of the glycine ^{13}C data. Thus, the amount of ATP^{4-} bound to Mn^{2+} was calculated from the stability constants in Table I. Further, it was assumed that the phosphate groups of only one ATP^{4-} are bound directly to Mn^{2+} as discussed in the Theoretical Models section and below in subsection E and that the relaxation rates of the ^{31}P nuclei of the remaining complex-bound ATP^{4-} molecules (one in $Mn(ATP)_2^{6-}$ and two in $Mn(ATP)_3^{10-}$, are practically unaffected by the Mn^{2+} ions. Consequently, the distances and the ligand exchange rate obtained in the analysis refer to one ATP^{4-} molecule per Mn^{2+} ion, only. Finally the rotational diffusion parameters (E_R, τ_R for $[ATP^{4-}]$ = 40 mM) found for the mixed glycine–Mn^{2+}–ATP^{4-} complexes on the basis of the glycine ^{13}C data were used as average values for the involved complexes. Thus, a somewhat smaller rate is expected for the $Mn(ATP)_3^{10-}$ complex, due to its larger molecular weight, while the almost equally populated species, $Mn(ATP)^{2-}$, may have a correlation rate that is somewhat faster and the less populated species, $Mn(ATP)_2^{6-}$, one that is slightly slower. The analysis thus performed results in the parameters in Table II. When the R_{1j} rate is calculated from eq 14 by using these parameters and the electron relaxation parameters in Table I, a scalar term is obtained which is negligible for any reasonable value of the ^{31}P electron hyperfine coupling constant ($A/\hbar < 10^8$ Hz);[19a,42] that is, $R_{1j}[^{31}P]$ is dominated exclusively by its dipolar term.

E. Stability, Structure, and Dynamics of the Binary Mn^{2+}–ATP^{4-} Complexes. Focusing first on the Mn^{2+}–ATP^{4-} interactions, the close agreement between the log K^{M}_{MA} (298 K) values obtained here (4.72 ± 0.07), and by potentiometric titrations in water solution[43] (4.78) under conditions where only $Mn(ATP)^{2-}$ is being formed, immediately suggests that the coordination of the first ATP^{4-} is identical in the two solvents; that is, the first ATP^{4-} binds directly to the Mn^{2+} and primarily through the phosphate moiety[24] as indicated in Figure 8. Yet, the enthalpy of formation, ΔH, observed here (−7.4 ± 1.4 kcal mol^{-1}) is numerically more than twice as large as the value in water[43] (−3.0 ± 0.3 kcal mol^{-1}). This, however, might well be due to the difference in solvent. Thus, the competition from water molecules for the positions in the first coordination sphere of the Mn^{2+} ions is undoubtedly smaller in the solvent applied here (water–glycerol 3:2, v/v) than in pure water, making the net loss in enthalpy associated with the Mn^{2+}–ATP^{4-} complexation larger. It should be noted in this context that the larger negative ΔH value found here could partly be due to an extra line broadening (R_{2p}) at the lower temperatures caused by the tangency of the Redfield limit (see section C).

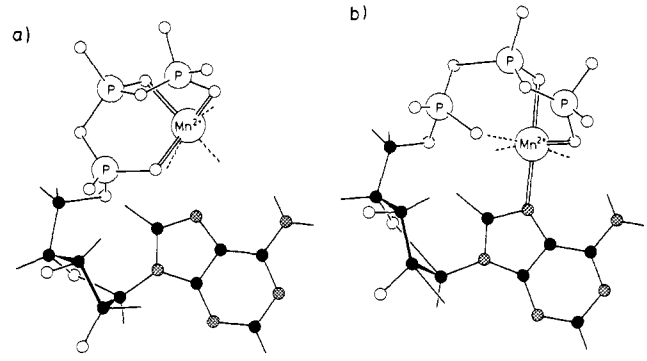

Figure 8. Possible structures for the $Mn(ATP)^{2-}$ complex. See text.

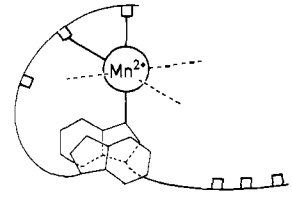

Figure 9. Possible structure for the $Mn(ATP)_2^{6-}$ complex. See text.

However, the physical reasonableness of the obtained log K^{M}_{MA} value seems to exclude any serious influence of this type.

Also the log $K^{MA}_{MA_2}$ value of 0.9 ± 0.15 mol^{-1} found here agrees with a value of about 1.0 mol^{-1}, previously estimated[20] for the $Mn(ATP)_2^{6-}$ complex in water at pD ≃ 7 on the basis of proton and phosphorus NMR line-width studies of the AMP^{2-}/ATP^{4-} competition for the Mn^{2+} ions and a value of 1.32 ± 0.06 mol^{-1} for the corresponding $Ni(ATP)_2^{6-}$ complex in water at pD 5.5, derived[25] from proton NMR chemical shifts. The suggestion[20] that the large difference between K^{M}_{MA} and $K^{MA}_{MA_2}$ reflects a significant difference in binding of the first and the second ATP^{4-} molecule in $Mn(ATP)_2^{6-}$ is further supported here by the difference in magnitude and sign of the ΔH^{M}_{MA} and $\Delta H^{MA}_{MA_2}$ parameters (Table I), although the uncertainty of the latter is too large to justify a quantitative interpretation.

The original proposal[20] that the binding of the second ATP^{4-} in the $Mn(ATP)_2^{6-}$ complex involves stacking of the two adenine rings with the two phosphate moiety as far apart as possible seems unchallenged. Likewise, the suggestion that the second ATP^{4-} coordinates only through its adenine ring agrees with studies of other ATP^{4-}–metal complexes[25,28] and of the ADP/Mn^{2+} system.[44] However, on the basis of the latter ^{17}O NMR study, and the size of the hyperfine coupling between the unpaired Ni^{2+} electrons and the adenine H(8) proton[21] in the ATP/Ni^{2+} system, it has been convincingly advocated[24] that the adenine N(7) coordinates directly to the metal ion, that is, without a bridging water molecule as proposed originally.[20,21] Supporting evidence for this conclusion is provided by ^{13}C relaxation studies of the ATP/Mn^{2+} system[22] and by recent ^{15}N relaxation studies of the AMP/Mn^{2+} system,[45] both at high ligand/Mn^{2+} ratios. Hence, a structure as sketched in Figure 9 seems most likely. However, a structure in which the second ATP^{4-} binds to the complex only through its stacking interaction with the phosphate-bound ATP^{4-}, while the latter forms a macrochelate through an *intra*molecular N(7) coordination (Figure 8b), also agrees with all the results mentioned. As for the specific stacking arrangement of the two adenine rings, the one shown in Figure 9 agrees with model building, and with the stacking arrangement of $Na_2H_2(ATP)$ in the crystal phase,[46] although an arrangement with a six-membered ring over a six-membered ring and a five-membered ring over a five-membered

(42) Mays, J. *Phys. Rev.* **1963**, *131*, 38–53.
(43) Taqui Khan, M. M.; Martell, A. E. *J. Am. Chem. Soc.* **1966**, *88*, 668–671.
(44) Zetter, M. S.; Lo, G. Y.-S.; Dodgen, H. W.; Hunt, J. P. *J. Am. Chem. Soc.* **1978**, *100*, 4430–4436.
(45) Levy, G. C.; Decther, J. J. *J. Am. Chem. Soc.* **1980**, *102*, 6191–6196.
(46) Kennard, O.; Isaacs, N. W.; Motherwell, W. D. S.; Coppola, J. C.; Wampler, D. L.; Larson, A. C.; Watson, D. G. *Proc. R. Soc. London, Ser. A* **1971**, *325*, 401–436.

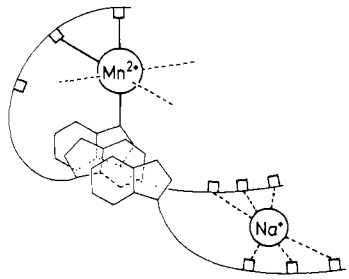

Figure 10. Possible structure for the $Mn(ATP)_3^{10-}$ complex. See text.

ring is also feasible according to model building. In this case the conformation about the glycosidic bond of the second ATP^{4-} must be syn in order for the phosphate moieties of the two ATP^{4-} to be as far apart as possible.

The most conspicuous result of the data analysis is the presence of the $Mn(ATP)_3^{10-}$ complex as indicated by the ATP^{4-} titration data (Figure 3). Apparently no report of this species has been given previously, neither in connection with NMR studies nor in connection with temperature-jump studies[47,48] of the Mn^{2+}/ATP^{4-} system at high ATP^{4-} and metal ion concentrations. This, however, seems reasonable considering the complexity of the system at high ligand and metal ion concentrations, which may easily result in a concealment of specific dependencies of the experimental data, unless an extensive and sufficiently versatile data set is applied. Thus, in the present study neither the variation of the measured glycine relaxation rates with temperature and field strength (Figure 1) nor the variation of the R_{2p} rate with the glycine concentration (Figure 2) gives any indication of the presence of the $Mn(ATP)_3^{10-}$ complex. On the contrary, the corresponding data fit a model in which this tris complex is neglected (case II). Only the ATP^{4-} titration data that cover more than 2 orders of magnitude in ATP^{4-} concentration provide the necessary information about the $Mn(ATP)_3^{10-}$ complex.

A similar stacking interaction as suggested for the binding of the second ATP^{4-} in $Mn(ATP)_2^{6-}$ can be envisaged for the binding of the third ATP^{4-} in $Mn(ATP)_3^{10-}$. Thus, as sketched in Figure 10, the adenine rings of the two loosely bound ATP^{4-} molecules may be placed parallel to each other and on each side of the adenine ring of the central, antiparallel ATP^{4-} molecule that is bound to the Mn^{2+} ion through its phosphate groups. Indeed, a similar stacking arrangement is found for $Na_2H_2(ATP)$ in the crystal phase.[46] On the other hand, model building clearly shows that the distance between the adenine rings of the two outer ATP^{4-} molecules ($\simeq$6.8 Å) excludes a simultaneous coordination of the adenine rings of both of these molecules. Therefore, only one of the two loosely bound ATP^{4-} can coordinate directly to Mn^{2+} if stacking of all three adenine rings shall be retained. Again, the possibility remains that both are bound only through stacking interactions to a central $Mn(ATP)^{2-}$–macrochelate. Nevertheless, the data analysis shows that the third ATP^{4-} binds more tightly to $Mn(ATP)_2^{6-}$ ($K^{MA_2}_{MA_3}$ = 112 ± 50 mol^{-1}) than does the second ATP^{4-} to $Mn(ATP)^{2-}$ ($K^{MA}_{MA_2}$ = 8 ± 3 mol^{-1}). This increased stability can be explained by a cooperative interaction between the second and the third ATP^{4-}, in that the base stacking in the tris complex is further stabilized by a weak Na^+ bridge between the phosphate moities of the two loosely coordinated ATP^{4-} molecules, as shown in Figure 10. Indeed, coordination of Na^+ to the phosphate groups of ATP^{4-} is observed[46] in the crystal structure of $Na_2H_2(ATP)$, just as it has been proposed[49] to play a salient role in the self-assembled structures of disodium guanosine 5′-monophosphate in water solution at neutral or slightly basic pH.

Additional details about the structure of the Mn^{2+}–ATP^{4-} complexes are obtained from the analysis of the $R_{1p}[^{31}P]$ rates (section D, Figure 7). First, the metal–phosphorus distances in Table II derived from these rates, assuming that only one ATP^{4-} molecule in each type of complex is coordinated to Mn^{2+} through its phosphate moiety, are well within the range of 2.8–3.8 Å required for a direct coordination[50-54] of the phosphate groups. In fact, the distances from the Mn^{2+} ion to the β and the γ phosphorus nuclei are, within the errors, identical with the value of 3.3 ± 0.1 Å derived[53] from the crystal structure[46] of Na_2H_2-(ATP) and Pauling ionic radii and from model building.[54] Therefore, the $R_{1p}[^{31}P]$ rates confirm that one of the ATP^{4-} molecules binds directly to the Mn^{2+} ion through its phosphate moiety, as already suggested by the large K^{M}_{MA} value. The agreement between the present $R_{1p}[^{31}P]$ data and the first coordination sphere interaction holds even if the correlation rate, τ_R^{-1}, applied here (see section D) should be slightly larger than the correct, average value. Thus, as judged from the composition and the molecular weight of the complexes involved, the applied correlation rate can hardly exceed the correct one by more than a factor of 2, which here will result in an increase of the distances of 11%. Hence, although the distances in Table II may be upper limits, they are still in agreement with a direct coordination. As for a possible delocalization of the unpaired Mn^{2+} electrons mediated by a direct covalent Mn^{2+}–^{31}P bond, such a delocalization could result in apparent distances that are too short. However, the agreement between the Mn^{2+}–^{31}P distances found here and those derived from crystal structures and model building suggests that the electron spin delocalization is insignificant. A similar conclusion has been reached previously for Mn^{2+}–carboxyl carbon interactions.[12-15]

In addition to the direct coordination of the phosphate moiety of one of the three ATP^{4-} in $Mn(ATP)_3^{10-}$, the data in Table II also reveal a distinct difference in distance between the Mn^{2+} ion and the β- and γ-phosphorus (3.32 ± 0.07 and 3.36 ± 0.05 Å) on one side and the Mn^{2+} and the α phosphorus (3.54 ± 0.05 Å) on the other side. Since the corresponding ratio between these distances, by and large, is independent of possible effects from the applied correlation rate, or electron spin delocalization, the observed difference in distance undoubtedly reflects a genuine difference in bonding. Immediately, this is suggestive of the intramolecular macrochelate formation (Figure 8b) reported for several divalent metal–ATP^{4-} complexes,[18-22,24,25,28,46,55-57] including $Mn(ATP)^{2-}$, for which macrochelate formation ranging from 10% to 38% has been reported.[24,28,57] Thus, the direct intramolecular coordination of the metal ion to N(7) that characterizes the macrochelates, excludes a first coordination sphere bonding to the α-phosphate[24] (Figure 8b), leaving only the β and γ groups of the phosphate moiety directly coordinated to the metal ion. However, despite the fact that the intramolecular macrochelate formations are concentration *in*dependent,[28] the data available here and in the literature[53] indicate that the observed bond-length ratio *increases* with the ATP^{4-} concentration, while at the same time the $Mn(ATP)^{2-}$ concentration decreases (see Figure 6). Thus here, a bond-length ratio of 3.33/3.54 is found for $[ATP^{4-}]$ = 0.040 M while a ratio of 3.3/3.7 was observed[53] for $[ATP^{4-}]$ = 0.1 M. Although somewhat different solvents were applied in the two cases, this comparison seems reasonable considering the close agreement between corresponding stability constants and the pK_a values in the two solvents. Also note that any influence here on the observed Mn^{2+}–phosphorus bond-length ratio due to the presence of the mixed-ligand complexes can be neglected because of the low concentrations of these complexes (see Figure 6).

(47) Hammes, G. G.; Miller, D. L. *J. Chem. Phys.* **1967**, *46*, 1533–1534.
(48) Hammes, G. G.; Levison, S. A. *Biochemistry* **1964**, 1504–1506.
(49) Bouhoutsos-Brown, E.; Marshall, C. L.; Pinnavaia, T. L. *J. Am. Chem. Soc.* **1982**, *104*, 6576–6584.
(50) Geller, S.; Durand, J. L. *Acta Crystallogr.* **1960**, *13*, 325–331.
(51) Mildvan, A. S.; Grisham, C. M. In "Structure and Bonding"; Dunitz, J. D., Hemmerich, P., Holm, R. H., Ibers, J. A., Jørgensen, C. K., Neilands, J. B., Reinen, D., Williams, R. J. P., Eds.; Springer-Verlag: Heidelberg, 1974; Vol. 20, pp 1–21.
(52) Sloan, D. L.; Mildvan, A. S. *J. Biol. Chem.* **1976**, *251*, 2412–2420.
(53) Brown, F. F.; Campbell, I. D.; Henson, R.; Hirst, C. W. J.; Richards, R. E. *Eur. J. Biochem.* **1973**, *38*, 54–58.
(54) Sundaralingam, M. *Biopolymers* **1969**, *7*, 821–860.
(55) Szent-Györgyi, A. "Bioenergetics"; Academic Press: New York, 1957; pp 64–73.
(56) Kuntz, G. P. P.; Glassman, T. A.; Cooper, C.; Swift, T. J. *Biochemistry* **1972**, *11*, 538–541.
(57) Mariam, Y. H.; Martin, R. B. *Inorg. Chim. Acta* **1979**, *35*, 23–28.

In order to account for the decreasing coordination of the α phosphate group with increasing [ATP^{4-}], the bis and tris ATP^{4-}–Mn^{2+} complexes must be considered. Thus, unlike the $Mn(ATP)^{2-}$ concentration, the concentration of $Mn(ATP)_2^{6-}$, and in particular that of $Mn(ATP)_3^{10-}$, increases considerably in the ATP^{4-} concentration range from 0.005 to 0.1 M (Figure 6). Rather, therefore, the observed increase of the Mn^{2+}–α phosphorus distance with increasing ATP^{4-} concentration reflects that the formation of an *intra*molecular macrochelate between Mn^{2+} and the phosphate-bound ATP^{4-} is more favorable in $Mn(ATP)_3^{10-}$ and $Mn(ATP)_2^{6-}$ than in $Mn(ATP)^{2-}$. Alternatively, the longer Mn^{2+}–α-phosphorus distance is caused by a N(7) coordination of the Mn^{2+} ion to one of the two loosely bound ATP^{4-} molecules (Figures 9 and 10).

A quantitative evaluation of the increase of the α-phosphorus–Mn^{2+} distance with increasing ATP^{4-} concentration, based on the data available, indicates a close correlation between this distance and the amount of $Mn(ATP)_2^{6-}$ and $Mn(ATP)_3^{10-}$ complexes. Thus, assuming that the α-phosphate is excluded from a direct coordination only in these complexes, one can calculate the distance r_d between the Mn^{2+} ion and the phosphorus in the displaced α-phosphate group, from the fraction, f, of the $Mn(ATP)_2^{6-}$ and the $Mn(ATP)_3^{10-}$ complexes at [ATP^{4-}] = 40 mM (f = 0.62) and the corresponding Mn^{2+}–β- and Mn^{2+}–α-phosphorus distances (3.34 and 3.54 Å, respectively; see Table II), using the equation $f/r_d^6 + (1-f)/3.34^6 = 1/3.54^6$. For f = 0.62, this yields r_d = 3.72 Å, that is, within the errors, the same as the value of 3.7 Å observed for [ATP^{4-}] = 0.10 M[53], where the bis and tris ATP^{4-}–Mn^{2+} complexes are almost totally dominating (f = 0.90), according to the stability constants in Table I. Although this agreement may be somewhat fortuitous, it further strengthens the suggestion that the observed exclusion of the α-phosphate from the first coordination sphere of the Mn^{2+} is associated primarily with the formation of the $Mn(ATP)_2^{6-}$ and the $Mn(ATP)_3^{10-}$ complexes.

The value of the rate, τ_{ATP}^{-1} (2.8×10^4 s^{-1} in Table I), of the exchange of the ATP^{4-} ligand that coordinates to Mn^{2+} through its phosphate moiety compares reasonably well with the rates for the same process in water, obtained by temperature-jump measurements[47,48] ($\simeq 10^4$ s^{-1}) and estimated in previous NMR studies through elaborate reasoning[20] (6×10^3 s^{-1}). However, since the exchange reaction may involve the water molecules,[3,58,59] the use of a glycerol–water solvent in the present study may render a direct comparison less meaningful. Thus, as indicated in the studies of the binary Mn^{2+}/glycine system in the same solvent,[15] the relatively low H_2O concentration as well as changes in the hydrogen bond interactions may give rise to slower ligand exchange rates in the glycerol–water solvent than in pure water.

F. Stability, Structure, and Dynamics of the Mixed Glycine–Mn^{2+}–ATP^{4-} Complexes. A suitable measure[1,2] of the tendency toward formation of mixed-ligand complexes is the difference in stability, $\Delta \log K$, between the binary and ternary complexes. Here, the difference $\Delta \log K = \log K_{MAG}^{MA} - \log K_{MG}^{M}$ corresponds to the equilibrium MA + MG $\rightleftarrows$ MAG + M, where A is ATP^{4-} and G is the average glycine species[15] that binds to Mn^{2+}. When the K_{MAG}^{MA} constant of Table I and the K_{MG}^{M} constant found previously are used,[15] $\Delta \log K$ takes the value of −0.9. Similarly, a value of −0.33 is obtained when the constant $\Delta \log K = \log K_{MAG}^{MA} - \log K_{MG}^{MG}$ is calculated, using a $K_{MG_2}^{MG}$ value[15] of 0.7 mol^{-1}. Clearly, these differences indicate that the coordination tendency of glycine toward $Mn(ATP)^{2-}$ is smaller than toward Mn^{2+} and the average Mn^{2+}–glycine monocomplex.[15]

When large surpluses of ligands are employed, as in the present study, it might be more appropriate[58] to describe the formation tendency of the mixed complexes by the constant $\log x = (\log K_{MGA}^{MG} - \log K_{MA_2}^{MA}) + (\log K_{MAG}^{MA} - \log K_{MG_2}^{MG})$, corresponding to the equilibrium $MA_2 + MG_2 \rightleftarrows 2MAG$. When $\log x$ is calculated from the K_{MA}^{M}, $K_{MA_2}^{MA}$, and K_{MAG}^{MA} constants in Table I and the K_{MG}^{M} and $K_{MG_2}^{MG}$ constants found previously,[15] a value of 2.2 is obtained,

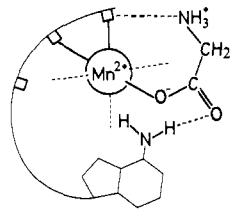

Figure 11. Possible structure for the mixed-ligand complex, Mn(ATP)(Gly)$^{6-}$. See text.

indicating a considerably larger tendency of mixed-ligand complex formation than may be expected for statistical reasons ($\log x \sim 0.6$).[2,58] Primarily, this increased tendency is due to the immense difference in magnitude of K_{MA}^{M} and $K_{MA_2}^{MA}$, a fact that stems from the difference in nature of the metal-binding of the two ATP^{4-} ligands, discussed above.

A more detailed description of the Mn^{2+}–ligand interactions than derivable from the stability constants is provided by the ^{13}C–Mn^{2+} distances, the ^{13}C-electron hyperfine coupling constant, and the ligand exchange rates, all obtained from the analysis of the relaxation data in sections B and D. First, the Mn^{2+}–C(1) distance (Table I) shows that the glycine carboxyl group in the mixed glycine–Mn^{2+}–ATP^{4-} complexes is bound directly to the Mn^{2+} ion. Thus, the obtained average value of 3.03 ± 0.10 Å is in accordance with the distance expected for such a bonding on the basis of the crystal structures[61] of divalent metal ion complexes of amino acids and peptides. Likewise, it agrees closely with the corresponding distances in the binary Mn^{2+}–glycine[15] and the Mn^{2+}–histidine[12] complexes. However, unlike the Mn^{2+}–glycine complexes observed in the corresponding binary system,[15] no appreciable fraction of the glycine in the mixed-ligand complexes has the amino group bound to the Mn^{2+} ion. Thus, the ratio of the R_{1p} rates of the two glycine carbons in the mixed glycine–Mn^{2+}–ATP^{4-} complexes, as obtained from the sample with the high ATP^{4-} concentration (40 mM), is only of the order of 1:3 in the entire fast-exchange temperature region. This corresponds to an average C(2)–Mn^{2+} distance > 3.6 Å when the distances are calculated from eq 14, using the correlation function obtained from the R_{1p} rates of C(1) (Table I) and the fraction of ligand-bound glycine derived from the R_{2p} data. For the sample with the low ATP^{4-} concentration (0.125 mM), the observed $R_{1p}C(2)/R_{1p}C(1)$ ratio is slightly larger than 1:3 and increases somewhat with temperature in the higher temperature region,[7] due to the significant amount of binary glycine–Mn^{2+} complexes that is present at that ATP^{4-} concentration (Figure 6), and which, furthermore, increases with temperature.[15] Clearly, these results exclude any significant amount of a direct glycine NH_2–Mn^{2+} bonding in the mixed glycine–Mn^{2+}–ATP^{4-} complexes, suggesting that only the carboxyl group coordinates to the Mn^{2+} ion. Hence, they agree with a single, well-defined, ternary complex as sketched in Figure 11. This agreement is further strengthened by the observation (Figure 1) that the R_{1p} rates of the glycine C(1) atom in the mixed-ligand complexes conform closely to the simple isotropic reorientation model implied by the Solomon model[31] (eq 14).

The difference between the glycine–Mn^{2+} interaction in the binary Mn^{2+}–glycine complexes and the mixed glycine–Mn^{2+}–ATP^{4-} complexes is further evidenced by a significantly larger value of the Mn^{2+}–C(1) electron–nucleus scalar coupling constant in the latter complex ($A/\hbar = (1.3 \pm 0.3) \times 10^6$ Hz; Table I) than in the former ($A/\hbar = (2.2 \pm 0.7) \times 10^5$ Hz).[15] Thus, the electron–carboxyl carbon coupling constant in transition-metal–amino acid complexes is *positive* when the coupling occurs through the carboxyl oxygens,[13] whereas it is *negative*[13,62] and numerically smaller when the coupling takes place through the amino group on the adjacent C(2) atom. Therefore, a detachment of the amino

(58) Sigel, H. *Angew. Chem., Int. Ed. Engl.* **1975**, *14*, 394–402.
(59) Eigen, M.; Tamm, K. *Z. Electrochim.* **1962**, *66*, 107–121.
(60) Jackopkin, L. G.; Yeager, E. B. *J. Phys. Chem.* **1970**, *74*, 3766–3772.
(61) Freeman, H. C. In "Advances in Protein Chemistry"; Anfinsen, C. B., Jr., Anson, M. L., Edsall, J. T., Richards, F. M., Eds.; Academic Press: New York, 1967; Vol. 22, pp 257–424.
(62) Strouse, C. E.; Matwiyoff, N. A. *J. Chem. Soc. D.* **1970**, 439–440.

group from the Mn^{2+} ion will result in a larger, positive value of $A/\hbar$[C(1)] as observed here, when the mixed glycine-Mn^{2+}-ATP^{4-} complex is compared with the corresponding binary glycine-Mn^{2+} complexes.

Finally the difference in the Mn^{2+}-NH_2 interaction of the binary and mixed-ligand complexes, just derived from the R_{1p} relaxation rates and the electron-nucleus hyperfine coupling, is paralleled by a difference in the glycine-ligand exchange rate which increases from $\tau_{MG}^{-1} = (3.9 \pm 1.2) \times 10^6$ s^{-1} and $\tau_{MG_2}^{-1} = (3.8 \pm 1.2) \times 10^6$ s^{-1} for the binary glycine complexes[15] to $\tau_{MAG}^{-1} = (7.8 \pm 1.5) \times 10^6$ s^{-1} in the ternary glycine-Mn^{2+}-ATP^{4-} complexes, all values referring to a temperature of 298 K. Again, this difference in exchange rates confirms the destabilizing effect of ATP^{4-} on the Mn^{2+}-glycine interaction.

According to model building, the difference between the glycine-Mn^{2+} interactions in the binary and the mixed-ligand complexes, thus established, can hardly be caused by steric hindrance. Rather, it is due to a direct interaction of the glycine with the ATP^{4-} ligand, most likely a polar interaction[4] between the positively charged ammonium group of the amino acid and the negatively charged phosphate groups of the nucleotide or a hydrogen bond between the carboxyl oxygen of the amino acid and the NH_2 group at the C(6) carbon of the adenine ring or a combination of such interactions as indicated in Figure 11. Both of these interactions may bring the two ligands in specific positions, or states, that are favorable for further reactions in enzymatic processes, in which they serve as substrates.

Conclusion

The present study shows that NMR relaxation studies can provide detailed information about the stability, structure, dynamics, and ligand exchange of paramagnetic metal complexes in solution, even in the case of a relatively complex system as the ternary glycine/Mn^{2+}/ATP^{4-} system investigated here. In particular, the study emphasizes the different glycine-Mn^{2+} interaction in the ternary glycine-Mn^{2+}-ATP^{4-} complexes and the binary glycine-Mn^{2+} complexes. Likewise, it reconciles the apparently conflicting results obtained previously[18-24,28,47] for systems with highly different values of the Mn^{2+}/ATP^{4-} ratio, by clarifying the difference in nature of the binary Mn^{2+}-ATP^{4-} complexes that dominate at these extremes.

The study also demonstrates that the paramagnetic relaxation of the ligand nuclei and the relaxation of the unpaired electrons of the Mn^{2+} complexes investigated can be described satisfactorily by the Solomon-Bloembergen-Morgan theories. This holds even if the Redfield limit for the spin-spin relaxation of the ligand nuclei is touched in part of the experimental region.

However, the data analyses strongly emphasize the necessity of providing a sufficiently versatile set of experimental data in order to obtain correct and unambiguous results. Hence, the experimental conditions must be varied over a range sufficiently large to allow each one of the involved parameters to influence the data set. This is clearly illustrated by the present analyses, where the tris complex, $Mn(ATP)_3^{10-}$, that reconciles the relaxation data obtained at the highly different Mn^{2+}/ATP^{4-} ratios is revealed only when the precise dependence of the relaxation rates on the ATP^{4-} concentration is incorporated in the data analysis.

Acknowledgment. I thank the Danish Natural Science Research Council for support of the Bruker HX 270 and WH 90 spectrometers and the JEOL FX 90Q spectrometer used here, as well as grant (J. 11-1819) for extra accessories. Free access to the RC computers at the H. C. Ørsted Institute and the least-squares program FUNCFIT by G. O. Sørensen is also gratefully acknowledged.

Registry No. P, 7723-14-0.

Supplementary Material Available: Tables (Tables III-VIII) containing the experimental R_{ka}, $R_{k,obsd}$, and R_{kp} data corresponding to Figure 1, 2, 3, and 8, (9 pages). Ordering information is given on any current masthead page.

Tandem Mass Spectrometry Methodology for the Sequence Determination of Cyclic Peptides

Klaus Eckart,[†] Helmut Schwarz,*[†] Kenneth B. Tomer,[‡] and Michael L. Gross*[‡]

Contribution from the Institut für Organische Chemie der Technischen Universität, D-1000 Berlin 12, West Germany, and the Midwest Center for Mass Spectrometry, Department of Chemistry, University of Nebraska—Lincoln, Lincoln, Nebraska 68588.
Received April 3, 1985

Abstract: The unequivocal sequence determination of cyclic penta- and hexapeptides, including biologically active enkephaline and somatostatine analogues, is achieved by using the following procedure. Production of gas-phase $[M + H]^+$ by using fast atom bombardment is followed by investigating either unimolecular or collision-induced dissociations of mass selected $[M + H]^+$ and $[MH -$ amino acid residues$]^+$ fragments. The unimolecular and collisionally activated decompositions of these ions and of their fragments resulting from decarbonylation enable one to elucidate unequivocally the sequence of cyclic peptides. As an example, the sequence determination of an unknown synthetic enkephalin analogue is presented. The amount of sample required for the determination is in the range of 5-100 nmol. Unambiguous sequencing cannot normally be achieved by only analyzing the decompositions of $[M + H]^+$ ions.

Sequencing of linear peptides by using either classical Edman degradation or various mass spectrometric methods can be viewed as a nearly routine procedure.[1-5] In distinct contrast, sequencing of cyclic peptides by means of the classical techniques is much more difficult because, except for special cases, chemical degradation via selective hydrolysis of specific peptide bonds is difficult to achieve. Unspecific hydrolysis followed by gas chromatogra-

[†] Institut für Organische Chemie der Technischen Universität.
[‡] University of Nebraska—Lincoln.

(1) Biemann, K. In "Biochemical Applications of Mass Spectrometry"; Waller, G. R., Dermer, O. C., Eds., Wiley: New York, 1980; p 469.
(2) Morris, H. R. *Nature (London)* **1980**, *286*, 447.
(3) Williams, D. H.; Bradley, C.; Bojesen, G.; Santikarn, S.; Taylor, L. C. E. *J. Am. Chem. Soc.* **1981**, *103*, 5700.

0002-7863/85/1507-6765$01.50/0